FERMILAB-PUB-77-139-E

IC/HENP/77/1

#418. See also Preprint file

Nuclear Size Dependence of Inclusive Particle Production*

D.A. Garbutt, R.W. Rusack, Ion Siotis.
Imperial College, London SW7 2AZ, United Kingdom.

and

D. Gross, D. Nitz, S. Olsen.**
University of Rochester, Rochester, New York 14627, USA.

and

K. Abe, R. Bomberowitz, K. Cohen, P. Goldhagen,
F. Sannes, D. Saroff, J. Willison.
Rutgers University, New Jersey 08903, USA.

ABSTRACT

The inclusive production of π^+, π^-, K^+, K^-, p and $\bar{p}$ for protons incident on carbon and tungsten targets was studied at the Internal Target Area of the Fermilab. We assume an A^{α} dependence for the inclusive cross sections and report here on the variation of α with incident momentum, transverse momentum and particle species.

It has been well established that total cross sections of high energy hadrons on various nuclei are proportional to A^{α}, where A is the atomic number and $\alpha \simeq 0.7$[1]. This effect is naively described as resulting from the shielding of the interior of the nucleus by the surface and is dependent on the large strength of hadronic interactions. Weaker probes of the nucleus, such as leptons, have total cross sections more nearly proportional to A.

Two recent particle production experiments[2] reported on the atomic number dependence of inclusive hadron production at large transverse momentum P_t. The results, when fitted by a form $A^{\alpha(p_t)}$ showed values of α for all types of produced particle which exceed unity for $P_t > 2.0$ GeV/c. This surprising effect has led to considerable theoretical discussion in the recent literature[3].

In order to study the effect further we have performed an experiment at the Internal Target Area of the Fermi National Accelerator Laboratory in which we compare particle production from carbon and tungsten over a wide range of incident momenta, P_{inc}, from 50 GeV/c to 275 GeV/c and $0.2 \lesssim P_t \lesssim 2.35$ GeV/c.

The experimental apparatus is shown in Fig. 1. It consists of two small spectrometers viewing the same target but not in coincidence. While settings of the main spectrometer were changed to accept various particle types and momenta the second spectrometer detected

negative pions at one of two fixed momenta and was used as a monitor of the run to run variations of the relative carbon to tungsten targeting efficiency.

The main spectrometer was 15^{o} from the circulating proton beam. T_1 through T_6 were scintillation trigger counters ranging in size from 3mm x 9.5mm for T_1 to 5cm x 5cm for T_6. The magnet in the main spectrometer bent particles vertically with a maximum strength of 1.5 Tesla-meters. The back end of the spectrometer was set at a central vertical bend of 80 milliradians for runs with recoil momentum P_{lab} up to 6 GeV/c and at 37 milliradians for P_{lab} between 6 and 10 GeV/c. The scintillation counters, $T_{7,8,9}$ formed a vertical hodoscope which allowed a run to be subdivided according to P_{lab}. A differential Cerenkov counter, DC, and threshold Cerenkov counters, C_1 and C_2, allowed the pions, kaons and protons to be clearly identified. Over most of the momentum range particle identification was overdetermined allowing measurement of efficiencies and rejection ratios.

The monitor spectrometer was 12^{o} from the circulating proton beam. It consisted of scintillation counters, S_1 - S_5, a bending magnet, and a threshold Cerenkov counter, C. It was set to count 2 GeV/c negative pions during all the low-momentum runs of the main spectrometer and 4.5 GeV/c negative pions during the high-momentum runs.

An important special feature of the apparatus was the targeting arrangement. The target consisted of thin carbon and tungsten fibres mounted radially on a rotating wheel inside the main ring vacuum chamber. The wheel was 5cm in diameter, and the fibres extended 2.5 $\pm$ 0.03cm beyond its rim. The carbon fibres were on the opposite side of the wheel from the tungsten fibres. A signal sychronized with the 50 c.p.s. rotation of the wheel indicated which target material produced a given event. The carbon fibres were 8.44 $\pm$ .07 microns in diameter as measured with a microscope and had a density of 1.87 $\pm$ .05 g/cm^3 as determined by an electro-balance and by a sink-float technique. The tungsten fibres were 3.08 $\pm$ .07 microns in diameter and were assumed to have a density of 19.3 g/cm^3. This target allowed us to take data continuosly during the acceleration ramp of the synchrotron.

The use of only two target materials does not allow us to verify the A^{α} dependence. We have therefore assumed it to be true for each particle species at fixed P_{inc} and P_t [2] and report here on the variations of α with P_t, P_{inc}, and particle species. We have

$$\alpha = \ln \frac{(R_W/R_C)}{(A_W/A_C)}$$ where R_W/R_C is the ratio of rates from equal numbers of tungsten and carbon nuclei and A_W, A_C are the respective atomic numbers. Even though the 3μ tungsten fibres were so thin that they occasionally broke while the target was rotating in the main ring vacuum their tip could only extend about

a millimetre in the beam before producing excessive counting rates. Because of this and the fact that each fibre varied in length by a few tenths of a millimetre the relative amount of tungsten and carbon was uncertain. This uncertainty, which is energy dependent because of a small vertical movement and shrinking of the beam during the acceleration ramp, was estimated by studying particle production ratios as a function of target height. It was determined to be about $\pm$ 15%. This gave an overall uncertainty in α at each energy of $\pm$ 0.05. On the other hand the use of the 12^{o} monitor spectrometer enabled the determination of the variation of α with P_t at fixed energy with much better accuracy.

It should be noted that the data presented here have been obtained at a fixed laboratory angle, θ = 260mr. In the proton-nucleon centre of mass system and at a fixed incident energy this corresponds to a centre of mass angle θ^* which varies with P_t and depends on the produced particle mass. The relation between θ^* and P_t at 3 different P_{inc} is shown in figure 2. The same figure shows ΔY, the rapidity gap between target and recoil particle, as a function of P_t.

Figure 3 shows the value of α as a function of P_t for various particle species at 3 incident energies. In all cases the exponent rises above unity and continues rising at the highest P_t of 2.35 GeV/c. At fixed P_t α does not show any significant dependence on

P_{inc} although a 10% variation from 75 GeV/c to 250 GeV/c would be compatible with our overall uncertainty at each energy. At the highest P_t the value of α for a given particle approaches that of the corresponding antiparticle. This remains true for pions over the entire P_t range while for kaons and especially for protons the two diverge at lower P_t. For protons we observe a turnover around P_t = 0.7 GeV/c with α rising very rapidly as P_t decreases. The same behaviour seems to be true for pions although the rise is less dramatic and the turnover occurs around P_t = 0.4 GeV/c. Unfortunately we do not have data for kaons and antiprotons below P_t = 0.5 GeV/c.

The detailed behaviour of α reported here indicates a dependence on the produced particle species which does not follow any simple pattern. The turnover at low P_t may be related to the kinematics at fixed laboratory angle shown in figure 2. For example, α which is a function of P_t and particle species may also depend on centre of mass system variables such as

$$\theta^* \text{ or } x = \frac{2P_{11}^*}{\sqrt{s}} = (\tan\theta^*)^{-1}\frac{2P_t}{\sqrt{s}} .$$

However, any such dependence would also imply a variation of α with P_{inc} at fixed P_t. A more natural possibility would be that α depends on the rapidity gap between nuclear target and recoil particle. As can be seen from figure 2 this gap decreases with decreasing P_t and

the turnover in α at low P_t may reflect the onset of target fragmentation. The fact that the turnover for pions occurs at lower P_t and is less pronounced than for protons can be understood in terms of the different ΔY variation for pions and protons shown in figure 2. Finally, the value of P_t at which α goes through a minimum is independent of P_{inc}. In the above picture this implies that the rapidity gap over which target fragmentation is important does not depend on incident energy.

We wish to thank the staff of the Internal Target Area at the Fermilab and in particular Mr. Paul Kurylo who prepared the rotating fibre targets.

REFERENCES

*This work has been supported by the UK Science Research Council, the US Energy Research and Development Administration and the US National Science Foundation.

** A.P. Sloan Fellow

1. G. Bellettini et al., Nucl. Phys. 79, 609 (1966).
S.P. Denisov et al., Nucl. Phys. B61, 62 (1973).

2. J.W. Cronin et al., Phys. Rev. D11, 3105 (1975).
U. Becker et al., Phys. Rev. Lett. 37, 1731 (1976).

3. G. Farrar, Phys. Lett., 56B, 185 (1975).
J. Pumplin, E.D. Yen, Phys. Rev., D11, 1812 (1975).
P.V. Landshoff, J.C. Polkinghorne, D.M. Scott, Phys. Rev., D12, 3738 (1975).
L. Bertocchi in "High Energy Physics and Nuclear Structure," Sante Fe and Los Alamos 1975, AIP Conference Proc. 26.
J.H. Kuhn, Phys. Rev., D13, 2948 (1976).
S. Fredriksson, Nucl. Phys., B111, 167 (1976).
G. Berlad, A. Dar, G. Eilam, Technion preprint PH 76-87.
A. Krzywicki, Phys. Rev., D14, 152 (1976).

FIGURE CAPTIONS

Figure 1

Schematic view of the experimental arrangement.

Figure 2

On the left the production angle θ^* in the proton-nucleon centre of mass system as a function of P_t at 3 incident energies. On the right the rapitidy gap ΔY between produced particle and nuclear target. Broken lines are for pions, solid lines for protons.

Figure 3

The power α of the A dependence vs P_t for the six particle species at 3 incident energies.

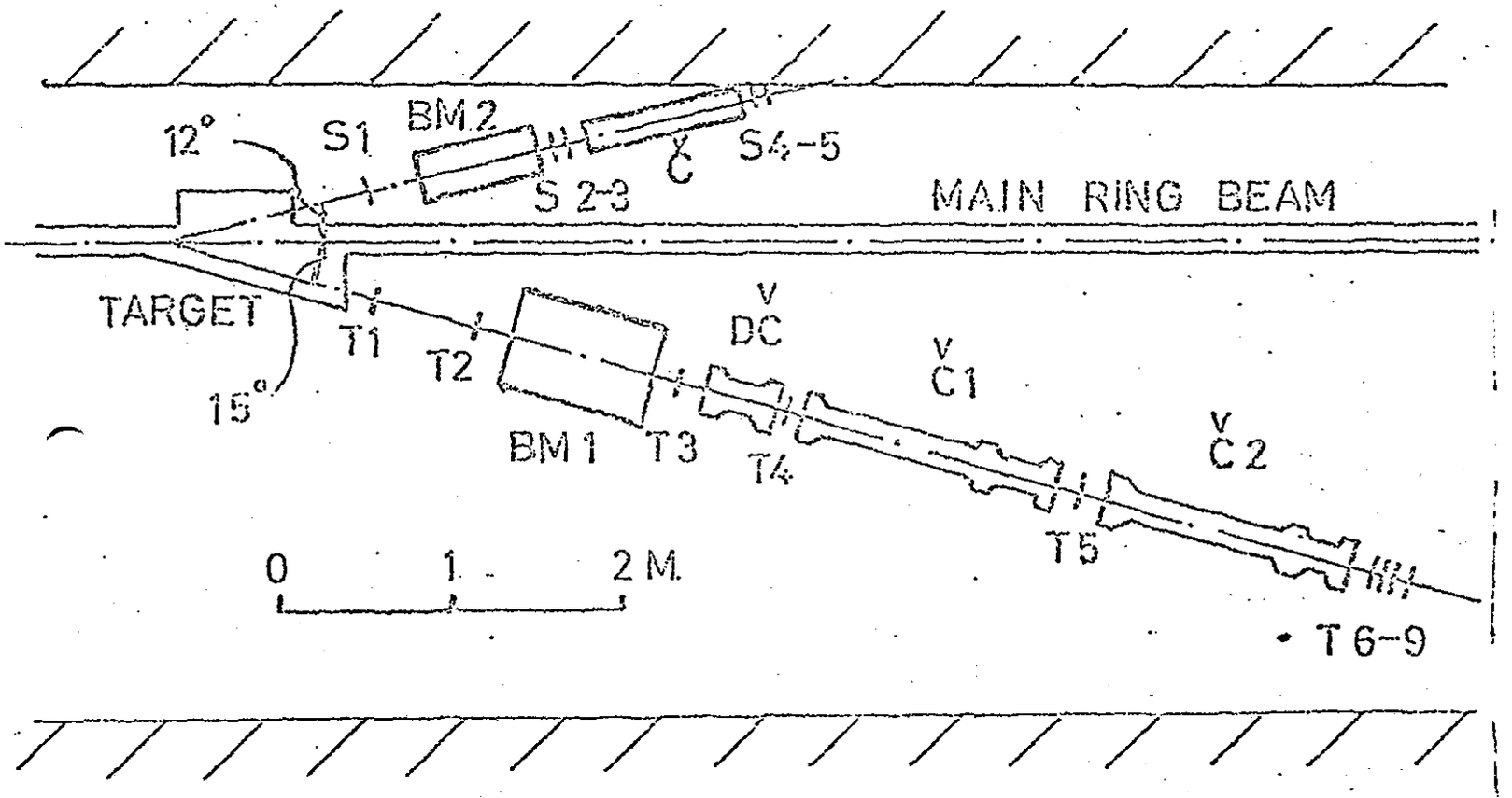
12°
S1
BM 2
S 2-3
S4-5
MAIN RING BEAM
TARGET
15°
T1
T2
BM 1
T3
DC
T4
C1
C2
T5
T6-9
0
1
2 M.

Fig. 1

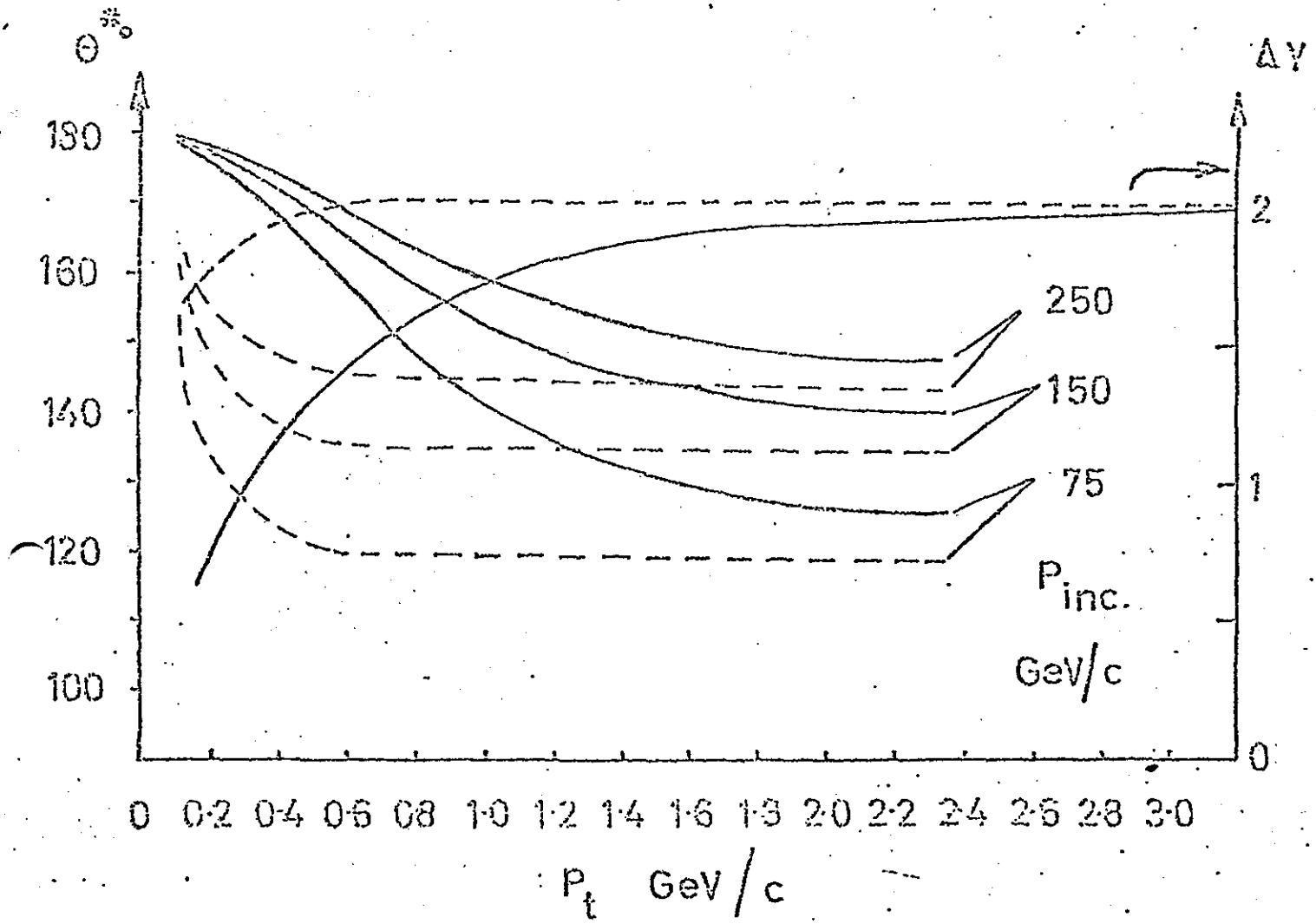
θ°
ΔY
180
160
140
120
100
2
1
0
250
150
75
P inc.
GeV/c
0 0·2 0·4 0·6 0·8 1·0 1·2 1·4 1·6 1·8 2·0 2·2 2·4 2·6 2·8 3·0
P t GeV/c

Fig. 2

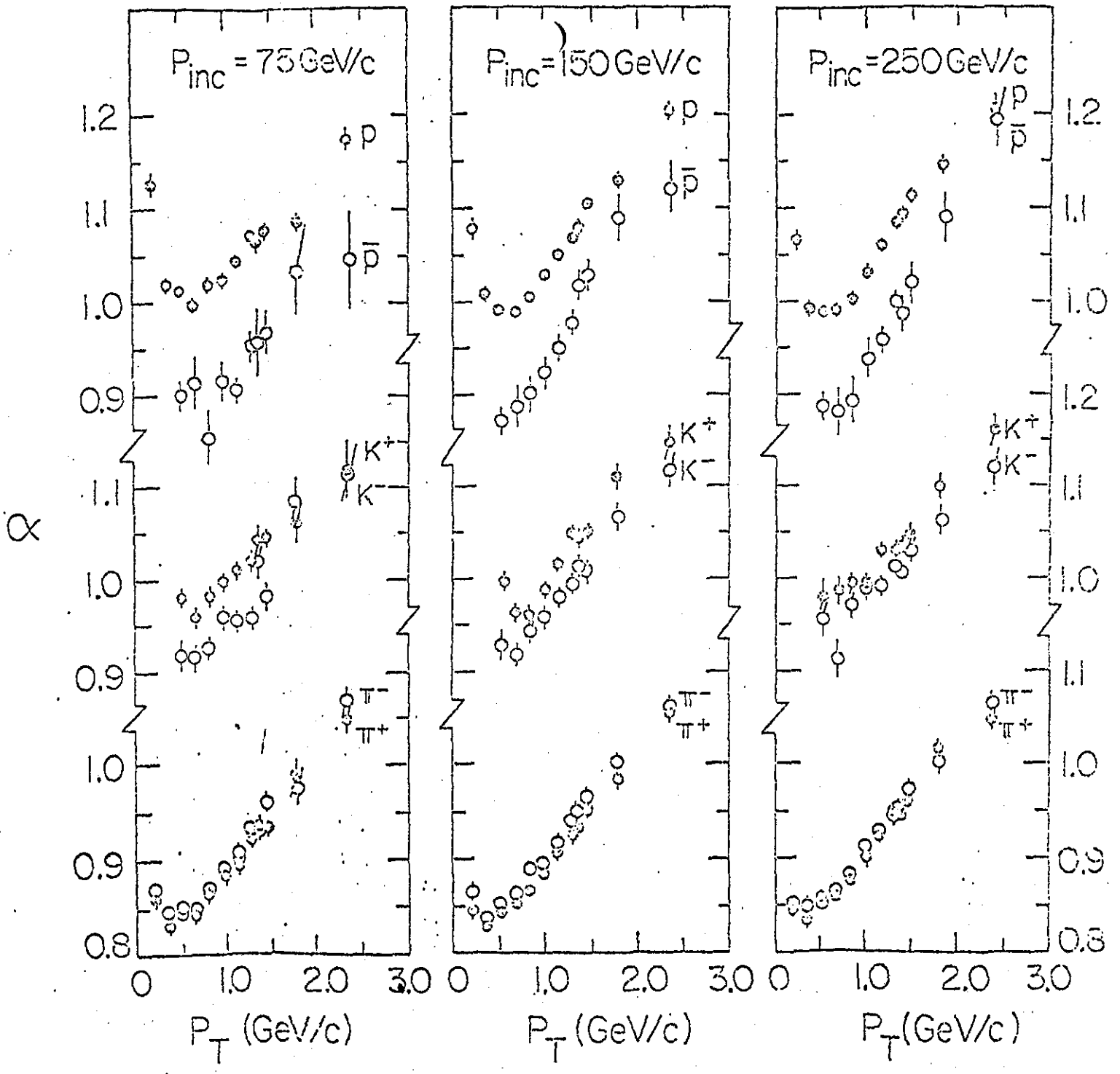
P_inc = 75 GeV/c
P_inc = 150 GeV/c
P_inc = 250 GeV/c
p
p̄
K+
K−
π−
π+
α
P_T (GeV/c)
P_T (GeV/c)
P_T (GeV/c)

Fig. 3.